Appl Phys B (2010) 98: 407–415
DOI 10.1007/s00340-009-3750-2

Applied Physics B
Lasers and Optics

Green luminescence and EPR studies on Mn-activated yttrium aluminum garnet phosphor

V. Singh · R.P.S. Chakradhar · J.L. Rao · H.-Y. Kwak

Received: 17 June 2009 / Revised version: 18 August 2009 / Published online: 3 October 2009

Abstract Yttrium aluminum garnet ($Y_3Al_5O_{12}$) and Mn activated $Y_3Al_5O_{12}$ phosphors have been prepared by urea combustion route in less than 5 min. The phosphors are well characterized by powder X-ray diffraction, Scanning electron microscopy and Fourier-transform infrared spectroscopic techniques. Photoluminescence tests on the pure $Y_3Al_5O_{12}$ showed a strong green emission at 525 nm (2.36 eV) attributed to the strongly allowed transition of F^+ center whereas in Mn^{2+} activated YAG the green emission at 519 nm is due to the $^4T_1$ (G) $\rightarrow$ $^6A_1$ (S) transition of Mn^{2+} ions. EPR studies have been carried out on Mn^{2+} activated $Y_3Al_5O_{12}$ phosphor at 300 and 110 K. From EPR spectra the spin-Hamiltonian parameters have been evaluated. The magnitude of the hyperfine splitting (A) indicates that the Mn^{2+} ions are in a moderately ionic environment. The spin concentration (N) and paramagnetic susceptibility (χ) have been evaluated and discussed.

PACS 78.55.-m · 33.35.+r · 32.50.+d · 76.30.-v

V. Singh (✉) · H.-Y. Kwak (✉)
Mechanical Engineering Department, Chung-Ang University, Seoul 156-756, Korea
e-mail: vijayjiin2006@yahoo.com

H.-Y. Kwak (✉)
e-mail: kwakh@cau.ac.kr

R.P.S. Chakradhar
Glass Technology Lab, Central Glass and Ceramic Research Institute, CSIR, Kolkata 700032, India

J.L. Rao
Department of Physics, Sri Venkateswara University, Tirupati 517 502, India

1 Introduction

Yttrium aluminum garnet ($Y_3Al_5O_{12}$, YAG) is a well known host for many rare-earth [1–3] and transition metal ions [4–6]. YAG based phosphors have been widely used in advanced optical technologies, solid-state laser, and fluorescent materials for luminescent applications [7–9]. These features have made YAG a relevant material for cathode-ray tubes (CRT), filed emission displays (FED), plasma display panel (PDP), scintillating and electroluminescent applications. Besides these properties, YAG has also been reported to possess good radiation storage properties that make it suitable for radiation dosimetry applications in ionizing radiation fields [10–12].

The synthesis, characterization and applications of rare earth-ion doped $Y_3Al_5O_{12}$ have been reported recently [13–16]. In the traditional method for the synthesis of aluminates, a solid state reaction procedure is employed, involving crushing, grinding and sintering at high temperature [17–19]. This is a cumbersome process. Therefore, new and effective synthesis methods are constantly tried. In this regard, we have successfully employed a combustion process for the synthesis of several alkaline earth aluminate phosphors [20–22]. In continuation of this interest, we have prepared YAG phosphor by a suitable combustion method and studied their luminescence properties.

Even though there are several studies on rare-earth ion doped YAG, studies on transition metal ion doped (especially Mn doped) YAG and undoped YAG are limited. Taking these points into account, we have synthesized $Y_{(3-x)}Mn_xAl_5O_{12}$ phosphor by the combustion method and characterized by X-ray diffraction (XRD), Fourier transform infrared spectroscopy (FT-IR), scanning electron microscopy (SEM) and Inductively coupled plasma mass spectrometry (ICP-MS) techniques. Electron paramagnetic reso-

nance (EPR) and Photoluminescence (PL) studies have also been carried out on the prepared phosphors and a mechanism of luminescence is proposed.

2 Experimental

2.1 Synthesis

Two phosphors, namely, $Y_3Al_5O_{12}$ [prepared using 5 g $Al(NO_3)_3{\cdot}9H_2O$, 3.0629 g $Y(NO_3)_3{\cdot}6H_2O$ and 3.2020 g CH_4N_2O] and $Y_{(3-x)}Mn_xAl_5O_{12}$, where $x = 0.01$ [prepared using 5 g $Al(NO_3)_3{\cdot}9H_2O$, 3.0527 g $Y(NO_3)_3{\cdot}6H_2O$, 3.2006 g CH_4N_2O, and 0.0052 g $MnCl_2{\cdot}4H_2O$] were prepared. All the reagents were of analytical grade purity. In a typical procedure, starting materials were mixed in an agate mortar to form a paste which was then transferred to a china dish and introduced into a muffle furnace maintained at 500 ± 10°C. As the dish was introduced, the combustion took place with the evolution of large amounts of gases. The escape of gases stopped after a few minutes of the introduction of the dish. During this period the contents of the dish boiled and formed froth which finally settled into a solid porous mass. The combustion was self-sustaining and self-terminated. The entire combustion process was completed in less than 5 min. The dish was then taken out, and the foamy product was crushed into a fine powder. This powder was used for its property characterization.

2.2 Characterization

Powder samples were analyzed for XRD using an X'Pert PRO-MRD, made in the Netherlands. It was used with Cu Kα radiation at 40 kV and 40 mA and a scan rate of 0.02°/s in the 2θ range from 10° to 70°. The data were collected using the X'Pert Data Collector data acquisition software, and were analyzed by means of the X'Pert HighScore data analysis package. FT-IR spectra were taken using a Perkin-Elmer Rx1 instrument in the range 4000–400 cm^{-1}. The morphology of the powders was obtained using a Hitachi S-4300 scanning electron microscope (SEM). EPR measurements were carried out using a Bruker EMX 10/12 X-band ESR spectrometer. Room temperature photoluminescence (PL) of the prepared phosphors was studied using a Hitachi F-4500 fluorescence spectrophotometer. Inductively coupled plasma mass spectrometry (ICP-MS) measurements were made with a VG Elemental PlasmaQuad 3 spectrometer.

3 Results and discussion

3.1 X-ray diffraction

Figures 1(A) and (B) show the X-ray diffraction patterns of pure $Y_3Al_5O_{12}$ powder and powder doped with Mn ions, respectively. It has been reported in the literature [23] that phase-pure YAG is not always achieved because the yttria–alumina system exhibits several other stable phases, including Y_2O_3, Al_2O_3, monoclinic $Y_4Al_2O_9$, metastable hexagonal $YAlO_3$, and orthorhombic $YAlO_3$. The X-ray diffraction patterns of both the doped and undoped samples indicate a dominant phase of $Y_3Al_5O_{12}$ with another secondary $YAlO_3$ phase. These patterns matched with those of standard $Y_3Al_5O_{12}$ (ICDD 88-2048) and $YAlO_3$ (ICDD 87-1288) (International Centre for Diffraction Data (ICDD)). Using the reference intensity ratio (RIR) [24], semi-quantitative analyses of the phase composition were done. It is clear from this analysis that our pure sample has 77% of $Y_3Al_5O_{12}$ and 23% of $YAlO_3$ phase [Inset (a) of Fig. 1(A)] while Mn doped sample has 96% of $Y_3Al_5O_{12}$ and 4% of $YAlO_3$ phase [Inset (b) of Fig. 1(B)]. The quantity of the secondary $YAlO_3$ phase was reduced due to the formation of vacancies resulting from the incorporation of Mn ions into the host lattice.

Kinetics of phase transformations in the Y_2O_3–Al_2O_3 system is strongly affected by the degree of crystallinity and homogeneity of the starting materials or by the presence of impurities and defects and was reported by several researchers [25–27]. Ullal et al. [28] have reported that the driving forces of nucleation for the YAG and $YAlO_3$ phases are quite comparable and one phase can become preferred when another phase is segregated. Besides, the impurities are also observed to influence the YAG formation, for example, nitrate compounds can easily induce $YAlO_3$ and carbon compounds promote YAG crystallization directly from the amorphous phase [28].

Recently, Yen-Pei Fu et al. [29] reported that both $Y_3Al_5O_{12}$ and $YAlO_3$ phases can be detected for Cr-doped amount from 1 to 3 mol%. Further increase of Cr-doped amount above 3 mol% for YAG:Cr powder led to the enhancement in the YAG diffraction peak intensity due to the improvement of crystallinity, and no $YAlO_3$ phase could be identified wherein the phosphors were synthesized using a microwave-induced combustion process with annealing temperature 1100°C for 2 h. Similar to this report [29], it is possible that Mn ions enhance the composition and crystallinity of the YAG and suppress the formation of $YAlO_3$.

3.2 FT-IR studies

The FT-IR spectra for both the doped and undoped samples (Fig. 2) show a broad band at around 3429 cm^{-1} and weak band at 1635 cm^{-1} which are characteristic of the stretching and bending modes of H_2O molecules. It was noticed that the weak band at about 1395 cm^{-1} is attributed due to the NO_3^- group, which might have come from the nitrate of the starting material [30]. For the doped sample, the depth of the absorption bands of NO_3^- decreased. The bands at 791 and 692 cm^{-1} represent the vibrations of Al−O, while the bands

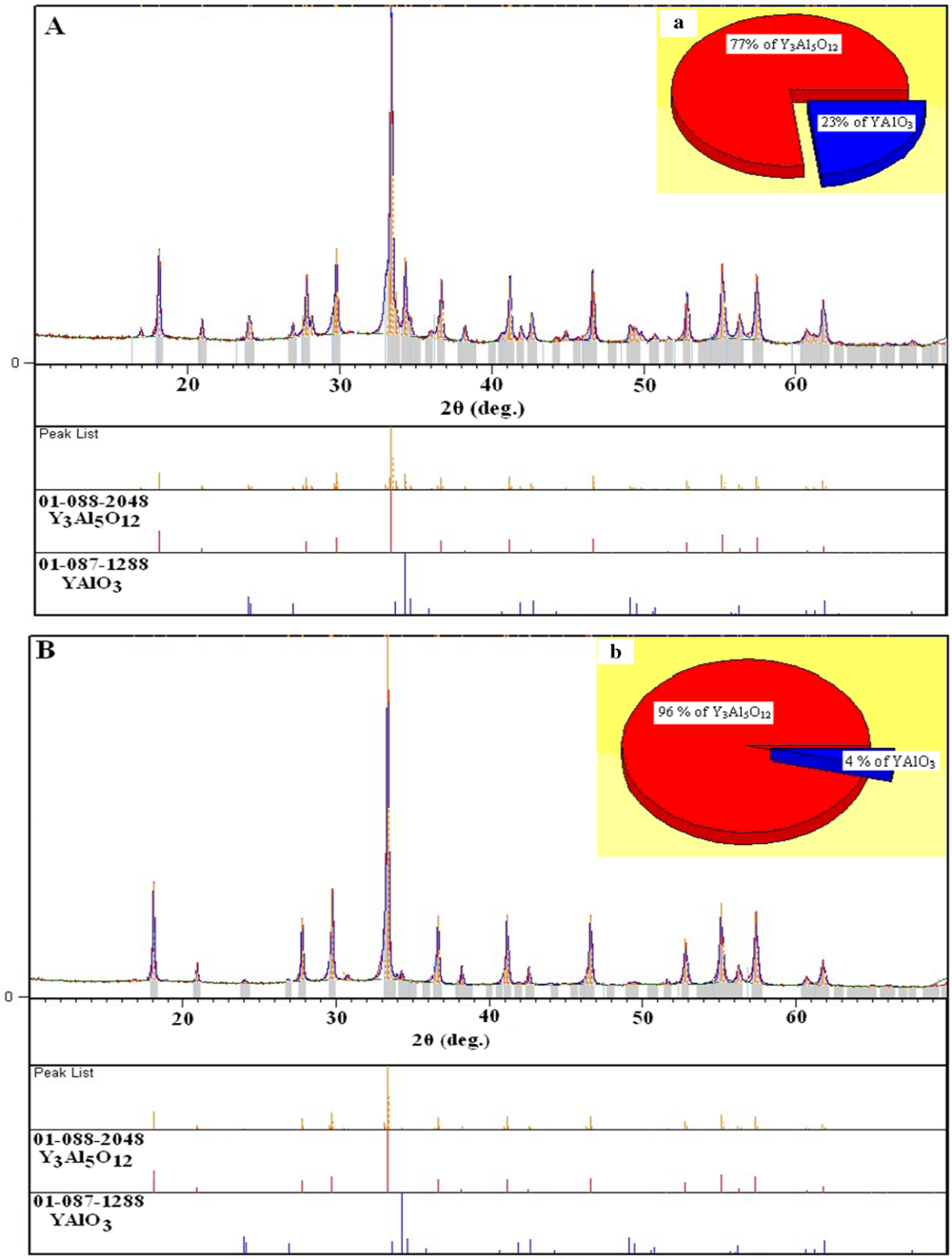

Fig. 1 XRD pattern of (**A**) $Y_3Al_5O_{12}$; inset (**a**) is the corresponding pie chart of semi-quantitative analysis. (**B**) XRD pattern of $Y_3Al_5O_{12}$:Mn; inset (**b**) is the corresponding pie chart of semi quantitative analysis

at 727, 568 and 463 cm^{-1} represent Y−O groups, both of which make up the YAG phase [31, 32]. For both the un-doped and doped samples, these bands are sharp, indicating a crystalline nature, and match with their XRD patterns.

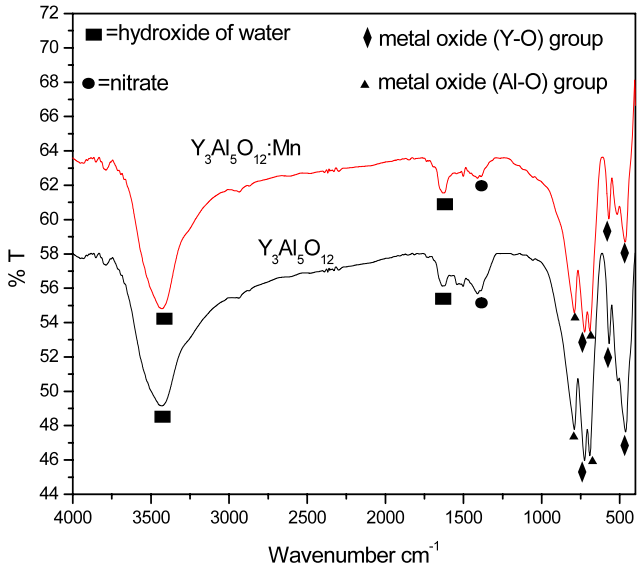

Fig. 2 FT-IR spectra of $Y_3Al_5O_{12}$ and $Y_3Al_5O_{12}$:Mn phosphor at room temperature

3.3 Scanning electron microscopy

Figures 3(A)–(D) and (E)–(H), show the SEM micrographs of undoped ($Y_3Al_5O_{12}$) and Mn doped ($Y_3Al_5O_{12}$:Mn) samples, respectively. The morphology of the undoped and doped powders remains mostly the same and consists of faceted crystals with apparent different sizes. Low resolution SEM micrographs show the crystals having apparently different sizes (Fig. 3(A) and (E)). Besides the faceted crystals, the powders show porous structure (Fig. 3(B)). During the combustion process, a large amount of gaseous material evolved, and hence the combustion product is porous. This porous structure is distributed non-uniformly in the matrix as some portions do not contain pores (Fig. 3(F)). This is believed to be related to the non-uniform distribution of temperature and mass flow in the combustion flame. In addition to these features, there also exist faceted crystals composed of very small crystals (Fig. 3(D)). Figures 3(G) and (H) are obtained respectively by magnifying portion (f) of Fig. 3(F) and (g) of Fig. 3(G). Carefully examining these surfaces under SEM, it is clear that they have sizes more than 250 nm.

3.4 Electron paramagnetic resonance studies

Figure 4 shows the EPR spectra of undoped YAG, which clearly shows that there are no paramagnetic impurities in the undoped sample. When Mn ions are introduced into YAG, the EPR spectra exhibit resonance signals characteristic of Mn^{2+} ions. Figure 5(a) shows the X-band EPR spectrum of $Y_{2.99}Mn_{0.01}Al_5O_{12}$ phosphor sample at room temperature. The spectrum at room temperature consists of three sets of resolved hyperfine structure, designated as a, b and c, centered around $g \approx 2.0$. Figure 5(b) shows the EPR spectrum of $Y_{2.99}Mn_{0.01}Al_5O_{12}$ phosphor at 110 K. The hyperfine structure originates from the interaction between the Mn^{2+} electron cloud and the ^{55}Mn nucleus (100% natural abundance) with the spin $I = 5/2$. The ability to observe the ^{55}Mn hyperfine structure has two tangible benefits: (1) it generally allows unambiguous assignments of positions of complex resonance lines to manganese; (2) the magnitude of hyperfine splitting constant (hfs) provides a measure of bonding between Mn^{2+} ion and its surrounding ligands [33, 34].

The electron configuration of Mn^{2+} ion is $3d^5$ (S state). In the case of d^5 metal ions, it is known that the axial distortion of octahedral symmetry gives rise to three Kramers doublets $|\pm 5/2\rangle$, $|\pm 3/2\rangle$ and $|\pm 1/2\rangle$ [35]. An application of Zeeman field will split the spin degeneracy of the Kramers doublets. As the crystal field splitting is normally much greater than the Zeeman field, the resonances observed are due to transitions within the Kramers doublets split by the Zeeman field. The resonance at $g \approx 2.0$ is due to Mn^{2+} ions in an environment close to an octahedral symmetry and is known to arise from the transition between the energy levels of the lower doublet $|\pm 1/2\rangle$.

The experimental results for the resonance fields can be analyzed with the usual spin-Hamiltonian [35]. From EPR, it is observed that the Mn^{2+} ion in the present study occupies more than one site. Also from XRD, it is noticed that, $Y_3Al_5O_{12}$ and $YAlO_3$ are the two common structures exhibited by the yttrium–alumina system. YAG is a cubic system of spinel structure whose space group is $Ia\bar{3}d$. It is commonly represented as $A_3[B_2C_3]O_{12}$, where A, B and C represent dodecahedral, octahedral and tetrahedral sites, respectively [36]. In the present case, A site is occupied by yttrium (ionic radius 1.019 Å), B and C sites are occupied by aluminum whose ionic radii are 0.67 Å and 0.53 Å in octahedral and tetrahedral sites, respectively. On the other hand, $YAlO_3$ belongs to orthorhombic perovskite structure with space group Pbnm [37]. In this, yttrium (ionic radius 1.019 Å) is in dodecahedral and aluminium (ionic radius 0.67 Å) occupies octahedral co-ordination. Since Mn^{2+} has an ionic radius of 0.96 Å, it is reasonable to assume that the manganese is occupying an yttrium site and the valence of manganese remains as Mn^{2+} as is evident from EPR and PL studies.

The calculated EPR spin-Hamiltonian parameters (g values and the hyperfine constants (A) for different sets a, b and c) are presented in Table 1. From the table, it is clear that the g values show a small anisotropy and deviate from the free electron value of 2.0023. It is known that an admixture of excited quartet levels into the ground state ^6S by spin orbit coupling produces a negative shift. A positive g shift observed arises due to electron transfer process through spin orbit interaction from ligand to S-state ion [38].

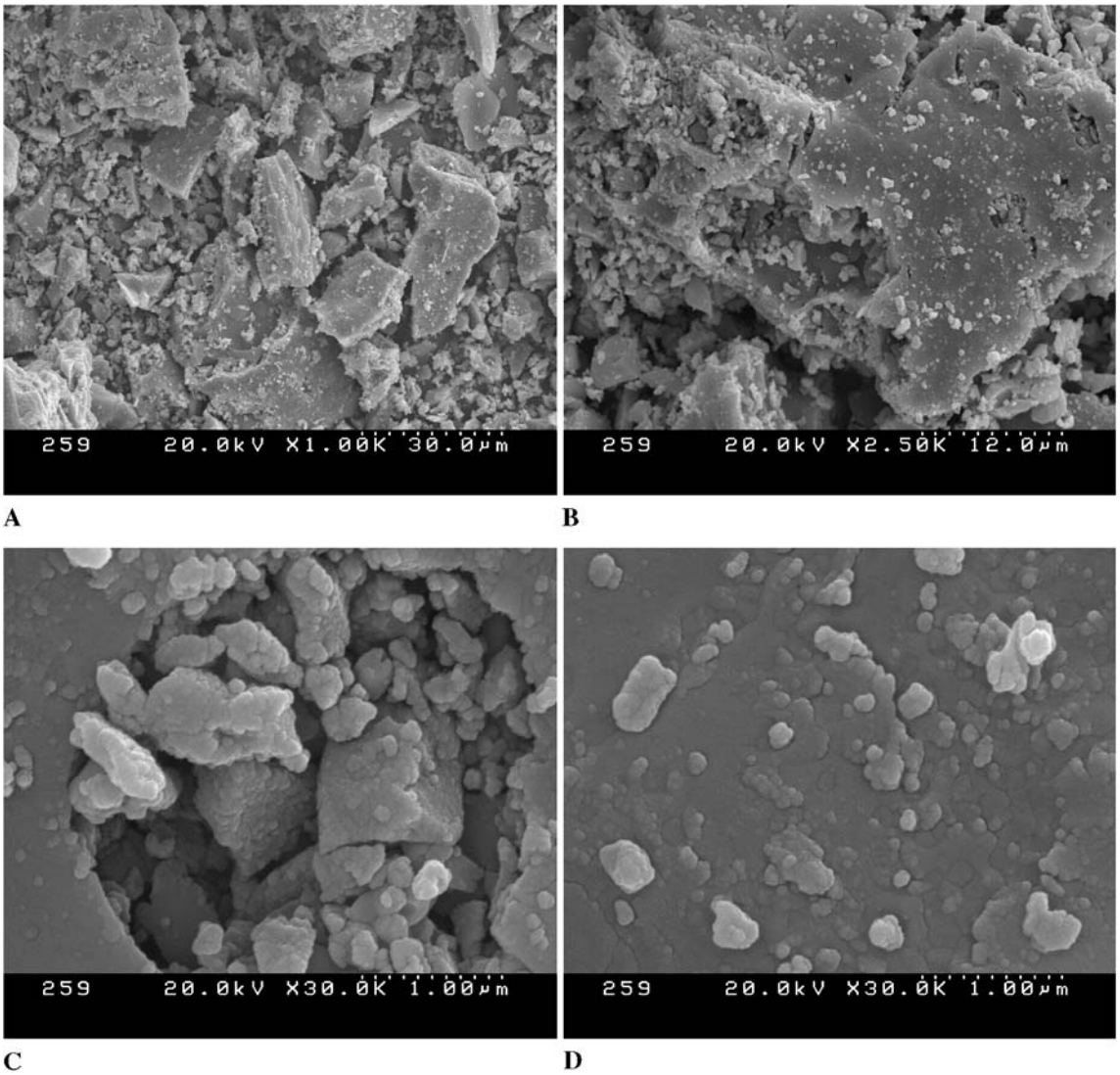

Fig. 3 SEM images of $Y_3Al_5O_{12}$ (**A**)–(**D**) and $Y_3Al_5O_{12}$:Mn phosphors (**E**)–(**H**)

The hyperfine splitting constant A of Mn^{2+} depends on the host lattice. This means that the magnitude of the hfs constant 'A' provides a qualitative measure of the ionicity of bonding between the Mn^{2+} ion and its ligands. 'A' was appreciably larger for ionic crystals than for covalently bonded ones [39]. Van Wieringen [33] empirically determined a positive correlation between 'A' and the ionicity of the manganese–ligand bond. On this basis, it is found that the bonding between Mn^{2+} ions and the surroundings in the present study is ionic ($A \approx 85$ G).

3.5 Calculation of number of spins (N) participating in resonance

The number of spins participating in resonance can be calculated by comparing the area under the absorption curve with that of a standard ($CuSO_4{\cdot}5H_2O$ in this study) of known concentration. Weil et al. [40] gave the following expression which includes the experimental parameters of both sample and standard:

$$N = \frac{A_x(\mathrm{Scan}_x)^2 G_{\mathrm{std}}(B_m)_{\mathrm{std}}(g_{\mathrm{std}})^2[S(S+1)]_{\mathrm{std}}(P_{\mathrm{std}})^{1/2}}{A_{\mathrm{std}}(\mathrm{Scan}_{\mathrm{std}})^2 G_x(B_m)_x(g_x)^2[S(S+1)]_x(P_x)^{1/2}}\,[\mathrm{Std}], \quad (1)$$

where A is the area under the absorption curve, which can be obtained by double integration of the first derivative EPR absorption curve, scan is the magnetic field corresponding to unit length of the chart, G is the gain, B_m is the modulation field width, g is the g-factor, S is the spin of the system in its ground state, P is the power of the microwave. The subscripts 'x' and 'std' represent the corresponding quantities for Mn^{2+} in $Y_{2.99}Mn_{0.01}Al_5O_{12}$ phosphor and the reference ($CuSO_4{\cdot}5H_2O$), respectively. The number of spins participating in resonance at $g \approx 2.0$ has been calculated at room

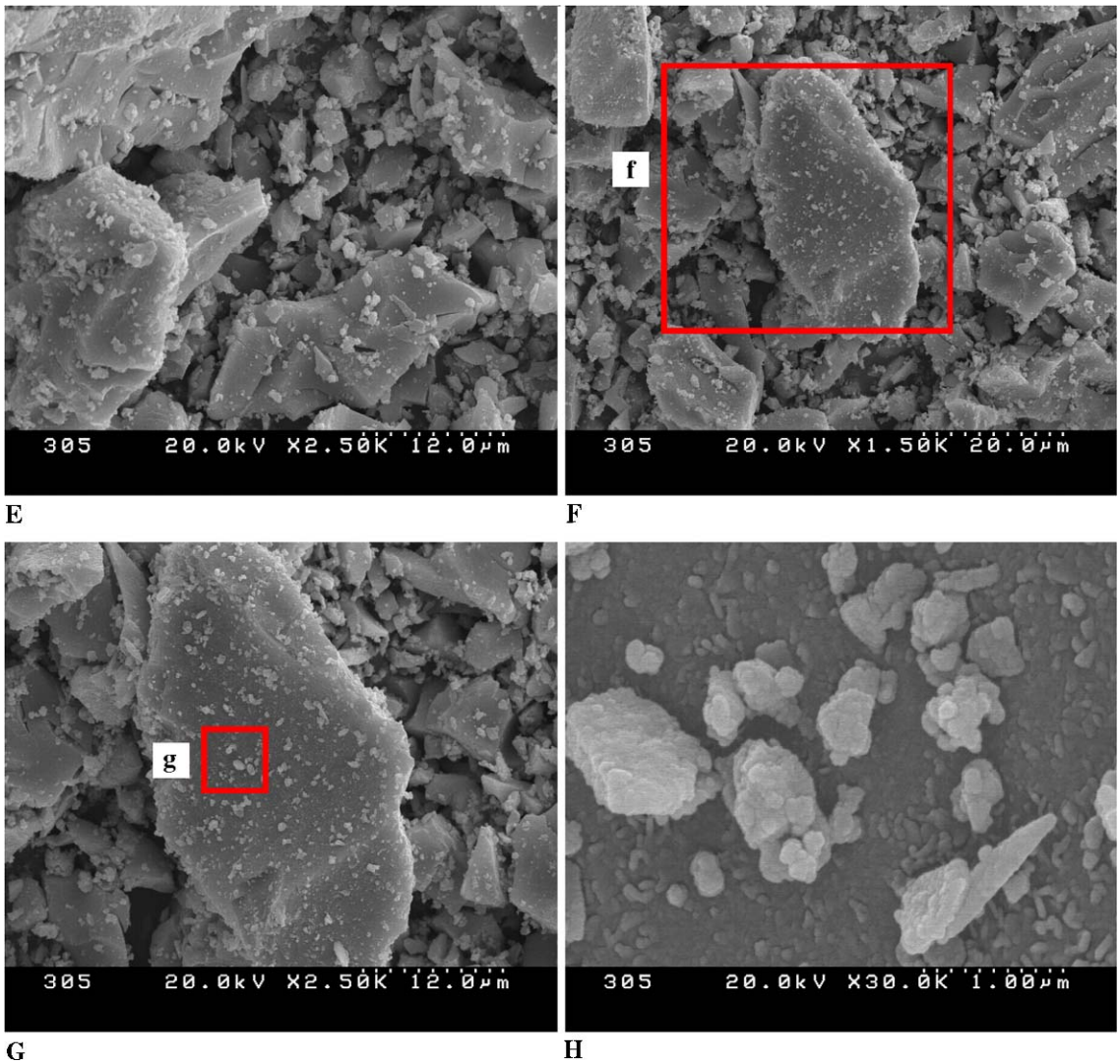

Fig. 3 (*Continued*)

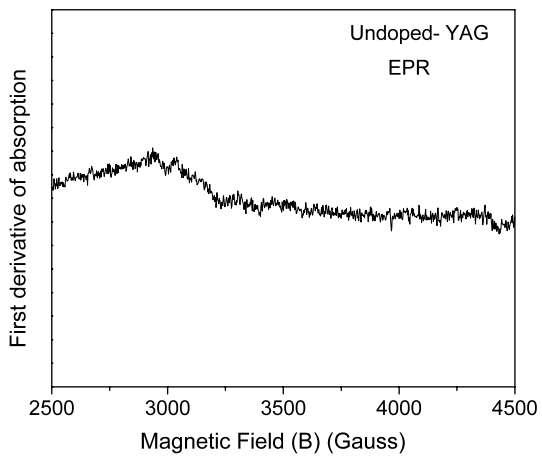

Fig. 4 EPR spectrum of the undoped $Y_3Al_5O_{12}$ phosphor at room temperature

temperature as well as at 110 K and is shown in Table 1. It is observed that as the temperature is lowered the number of spins increases, obeying the usual Boltzmann law.

3.6 Calculation of paramagnetic susceptibility (χ) from EPR data

The paramagnetic susceptibility can be calculated from EPR data using the formula [41]

$$\chi = \frac{Ng^2\beta^2 J(J+1)}{3k_B T}, \tag{2}$$

where 'N' is the number of spins per m^3, the other symbols have their usual meaning. The number of spins 'N' can be calculated by double integration of the first derivative EPR spectrum, and g is taken from EPR data. The paramagnetic

Table 1 The spin-Hamiltonian parameters, number of spins concentration (N) and paramagnetic susceptibility (χ) for $Y_3Al_5O_{12}$:Mn phosphors at room temperature and 110 K

System	Temperature (K)	g (± 0.001)	A_{avg} (gauss)	$N \times 10^{21}$ (arb. units)	$\chi \times 10^{-4}$ ($m^3\,kg^{-1}$)
$Y_3Al_5O_{12}$:Mn	300	$g_a = 2.005$	$A_a = 87$	0.41	1.02
		$g_b = 2.014$	$A_b = 83$		
		$g_c = 2.028$	$A_c = 84$		
$Y_3Al_5O_{12}$:Mn	110	$g = 2.007$	$A = 89$	1.43	3.51

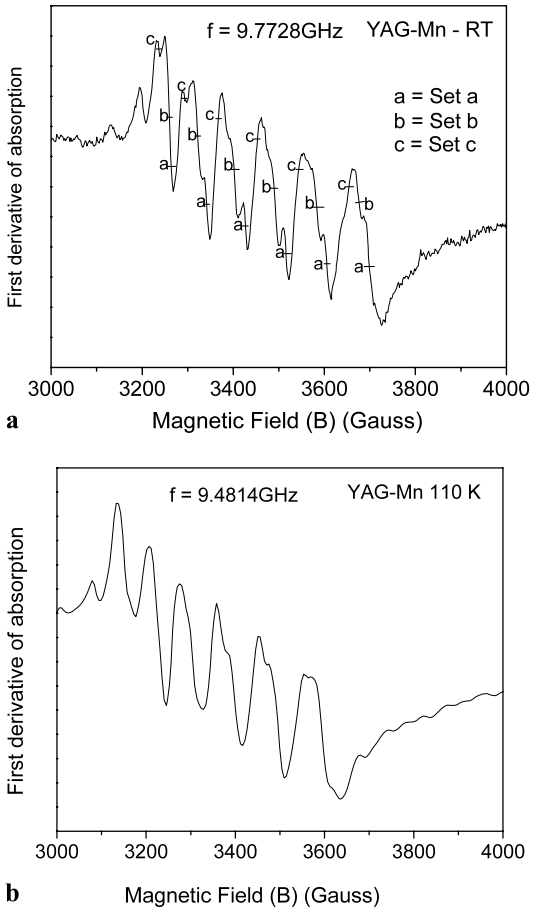

Fig. 5 (**a**) EPR spectrum of $Y_3Al_5O_{12}$:Mn phosphor at room temperature and (**b**) EPR spectrum of $Y_3Al_5O_{12}$:Mn phosphor at 110 K

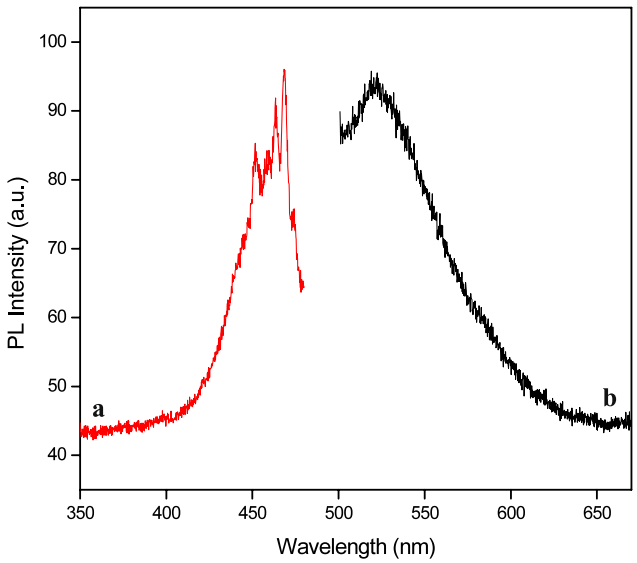

Fig. 6 Photoluminescence of $Y_3Al_5O_{12}$:Mn phosphor: (**a**) excitation spectrum ($\lambda_{em} = 519$ nm), (**b**) emission spectrum ($\lambda_{ex} = 468$ nm)

susceptibility has also been evaluated with respect to temperature and is presented in Table 1. It is observed that with increasing temperature the susceptibility of the sample decreases in accordance with N.

3.7 Photoluminescence studies

Figures 6(a) and (b) show the excitation and emission spectra of $Y_{2.99}Mn_{0.01}Al_5O_{12}$ phosphor at room temperature. The photoluminescence spectra of $Y_{2.99}Mn_{0.01}Al_5O_{12}$ indicate a green emission peak at 519 nm corresponding to the $^4T_{1g}$ (G) $\rightarrow$ $^6A_{1g}$ (S) transition of Mn^{2+} ions upon λ_{exc} 468 nm. The excitation spectrum corresponding to this emission shows peaks at 451, 458, 463, 468 nm. The observed bands are characterized by the transitions of $3d^5$ of Mn^{2+} ions acting as an activating center. In a cubic crystalline field of low to moderate strength, the five d electrons of Mn^{2+} ions are distributed in the t_{2g} and e_g orbitals, with three in the former and two in the latter. Thus the ground state configuration is $(t_{2g})^3(e_g)^2$. This configuration in octahedral symmetry (O_h) gives rise to the electronic states $^6A_{1g}$, $^4A_{1g}$, ^4E_g, $^4T_{1g}$ and to a number of doublet states of which $^6A_{1g}$ lies lowest according to Hund's rule. Since all the excited states of Mn^{2+} ion (belonging to d^5 configuration) will be either quartets or doublets, the luminescence spectra of Mn^{2+} ions will have only spin forbidden transitions. The emission at 519 nm is a typical green emission. The emission process from this material is attributed to a d-level spin-forbidden transition for the Mn^{2+} ions acting as an activating center. In particular, the transition from the lowest excited state to the ground state, $^4T_1$ to $^6A_1$, is directly responsible for the green light emission.

In the present study, we have also observed a strong green emission in undoped YAG phosphor. Initially, we irradiated the undoped powders, with UV lamp and noticed

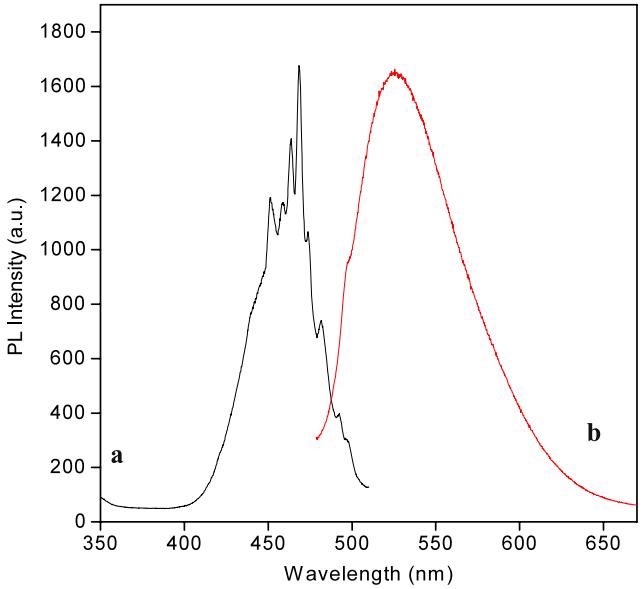

Fig. 7 Photoluminescence of the undoped $Y_3Al_5O_{12}$ phosphor: (**a**) excitation spectrum ($\lambda_{em} = 525$ nm), (**b**) emission spectrum ($\lambda_{ex} = 468$ nm)

that it emitted green light. In order to confirm this, later we recorded the PL spectrum of undoped YAG phosphor. Figures 7(a) and (b) respectively show the excitation and emission spectra of undoped YAG phosphor at room temperature. The photoluminescence spectrum of undoped YAG phosphor excited at 468 nm shows a strong green emission peak at 525 nm, compared to Mn^{2+} activated phosphor. The origin of green emission in this undoped phosphor is not clear; it may be due to the defect centers which are formed due to the thermal shock created by the high flame temperature. In order to make sure there are no paramagnetic impurities, we have also carried out chemical analysis using inductively coupled plasma mass spectrometry (ICP-MS). The results confirmed that no manganese was present in undoped YAG. Further, our EPR results also show that no Mn was present in the undoped sample. To confirm this result, we have prepared fresh samples again by using Aldrich chemicals, and in all the cases we observed a strong green emission in undoped YAG. Luminescence of this type cannot be ascribed to characteristic transitions of certain atoms or ions. The observation of green emission in undoped YAG might be due to anion defect center which might be formed during combustion process. As explained earlier, the YAG is a cubic system of spinel structure and the spinel structure is known to have the ability to accept structural vacancies, thus forming the defect [42, 43]. The close packing of oxygen in most spinels is not quite ideal. The highest intensity is speculated to result from the high concentration of oxygen vacancies in the lattices.

Relatively little is known about the origin of intrinsic defects in YAG. The theoretical [44] and experimental [45, 46] studies to identify the absorption band of F-type centers were undertaken. Adrichuk et al. [47] have reported a 2.38 eV emission band which can be created in garnet crystals by thermo-chemical treatment under reducing conditions designed to introduce a stoichometric excess of the metallic constituent, and hence anion vacancies. In the present study, we have observed a strong green emission at 525 nm (2.36 eV) in the undoped YAG compared to Mn^{2+}activated one. The emission at 2.36 eV is attributed to the associated defect in anion (oxygen) sub-lattice of YAG, i.e., the oxygen vacancy. Two types of centers relating to an anion vacancy are now known in oxide crystals [48, 49]: F^+-centers where one electron is trapped at the anion vacancy and F-centers where two electrons are trapped at the anion vacancy. Therefore, it is reasonable to assign this 2.36 eV emission in the undoped YAG to F^+-centers in this phosphor. Ashurov et al. [50] have also attributed the green emission to F^+centers in garnet crystals. This might be the possible reason for the strong green emission in the undoped YAG.

4 Conclusions

Green emitting YAG phosphor without any doping is produced by combustion synthesis. This involved furnace temperatures as low as 500°C and a very short time of 5 minutes. This seems to be an economical process for producing green emitting phosphors for several optoelectronic applications. This is attributed to the readymade formation of defect centers (F^+-centers) which are formed due to the thermal shock created by the high flame temperature. It is a unique feature of this synthesis method that these defect centers are promoted in the undoped $Y_3Al_5O_{12}$ phosphor. The green emission at 525 nm in undoped $Y_3Al_5O_{12}$ may correspond to the electron transition from deep oxygen vacancy level to the valance band. FT-IR analysis indicated the vibrations of metal–oxygen (M–O) groups which form the YAG phase. The high resolution SEM micrographs showed the presence of several small particles within the grains. The EPR study shows that the Mn^{2+} ion occupies more than one site. As per XRD and EPR, we can conclude that Mn^{2+} ions occupy yttria site of YAG. The magnitude of the hyperfine splitting (A) indicates that the Mn^{2+} ions are in moderately ionic environment. The number of spins participating in resonance (N) with temperature obeys the usual Boltzmann law. The paramagnetic susceptibility (χ) with temperature have also been evaluated. The green emission peak at 519 nm in Mn^{2+} activated $Y_3Al_5O_{12}$ is assigned to $^4T_{1g}$ (G) $\rightarrow$ $^6A_{1g}$ (S) transition of Mn^{2+} ions.

Acknowledgements Vijay Singh gratefully acknowledges Research Assistant Professorship at Chung-Ang University, Seoul (South Korea) from BK21 program. Another author (Dr. RPSC) is grateful to Dr. H.S. Maiti, Director, CGCRI and Dr. Ranjan Sen, Head, GTL lab, CGCRI for their constant support and encouragement.

References

1. C. Sanchez-Valle, I. Daniel, B. Reynard, R. Abraham, C. Goutaudier, J. Appl. Phys. **92**, 4349 (2002)
2. J.B. Gruber, B. Zandi, U.V. Valiev, Sh.A. Rakhimov, Phys. Rev. B **69**, 115103 (2004)
3. A. Potdevin, G. Chadeyron, D. Boyer, B. Caillier, R. Mahiou, J. Phys. D: Appl. Phys. **38**, 3251 (2005)
4. A. Ikesue, K. Yoshida, K. Kamata, J. Am. Ceram. Soc. **79**, 507 (1996)
5. G. Pari, A. Mookerjeea, A.K. Bhattacharyya, Physica B **358**, 7 (2005)
6. W.-C. Zheng, W. Fang, Y. Mei, J. Appl. Phys. **101**, 053911 (2007)
7. S. Shionoya, *Phosphor Hand Book* (CRC Press, Boca Raton, 1998), pp. 394 and 515
8. P. Schotler, R. Schmidt, J. Schneider, Appl. Phys. A **64**, 417 (1997)
9. T. Tamura, T. Setomoto, T. Taguchi, J. Lumin. **87–89**, 1180 (2000)
10. E. Zych, C. Brecher, H. Lingertat, J. Lumin. **78**, 121 (1998)
11. R.A. Rodrıguez-Rojas, E. De la Rosa-Cruz, L.A. Dıaz-Torres, P. Salas, R. Melendrez, M. Barboza-Flores, M.A. Meneses-Nava, O. Barbosa-Garcıa, Opt. Mater. **25**, 285 (2004)
12. E. De la Rosa, R.A. Rodrıguez, R. Melendrez, P. Salas, L.A. Diaz-Torres, M. Barboza-Flores, Nucl. Instrum. Methods Phys. Res., Sect. B **255**, 357 (2007)
13. A. Potdevin, G. Chadeyron, D. Boyer, R. Mahiou, J. Non-Cryst. Solids **352**, 2510 (2006)
14. G. Xia, S. Zhou, J. Zhang, S. Wang, J. Xu, J. Alloys Compd. **421**, 294 (2006)
15. H. Yagi, T. Yanagitani, H. Yoshida, M. Nakatsuka, K. Ueda, Opt. Laser Technol. **39**, 1295 (2007)
16. J.-H. In, H.-C. Lee, M.-J. Yoon, K.-K. Lee, J.-W. Lee, C.-H. Lee, J. Supercrit. Fluids **40**, 389 (2007)
17. D.R. Meisser, G.E. Gazza, Am. Ceram. Soc. Bull. **51**, 692 (1972)
18. A. Ikesue, I. Furusato, K. Kamata, J. Am. Ceram. Soc. **78**, 225 (1995)
19. A. Ikesue, T. Kinoshita, K. Kamata, K. Yoskida, J. Am. Ceram. Soc. **78**, 1033 (1995)
20. V. Singh, T.K. Gundu Rao, J.-J. Zhu, J. Solid State Chem. **179**, 2574 (2006)
21. V. Singh, T.K. Gundu Rao, J.-J. Zhu, J. Lumin. **126**, 1 (2007)
22. V. Singh, V. Natarajan, J.-J. Zhu, Opt. Mater. **29**, 1447 (2007)
23. B. Cockayne, J. Less-Common Met. **114**, 199 (1985)
24. C.R. Hubbard, R.L. Snyder, Powder Diffr. **3**, 74 (1988)
25. Y. Iida, A. Towata, T. Tsugoshi, M. Furukawa, Vibr. Spectrosc. **19**, 399 (1999)
26. C.N.R. Rao, J. Gopalakrishnan, *New Directions in Solid State Chemistry* (Cambridge University Press, Cambridge, 1997)
27. M. Gervais, S. Le Floch, N. Gauthier, D. Massiot, J.P. Coutures, Mater. Sci. Eng. B **45**, 108 (1997)
28. C.K. Ullal, K.R. Balasubramaniam, A.S. Gandhi, V. Jayaram, Acta Mater. **49**, 2691 (2001)
29. Y.-P. Fu, S. Tsao, C.-T. Hu, J. Alloys Compd. **395**, 227 (2005)
30. V. Sarawati, G.V.N. Rao, G.V. Rama Rao, J. Mater. Sci. **22**, 2529 (1987)
31. I. Muliuoliene, S. Mathur, D. Jasaitis, H. Shen, V. Sivakov, R. Rapalaviciute, A. Beganskiene, A. Kareiva, Opt. Mater. **22**, 241 (2003)
32. Y. Zhou, J. Lin, M. Yu, S. Wang, H. Zhang, Mater. Lett. **56**, 628 (2002)
33. J.S. van Wieringen, Discuss. Faraday Soc. **19**, 118 (1955)
34. F.D. Tsay, L. Helmholz, J. Chem. Phys. **50**, 2642 (1969)
35. A. Abragam, B. Bleaney, *Electron Paramagnetic Resonance of Transition Ions* (Clarendon, Oxford, 1970)
36. H. Yagi, K. Takaichi, K.-i. Ueda, T. Yanagitani, A.A. Kaminskii, Opt. Mater. **29**, 392 (2006)
37. R. Diehl, G. Brant, Mater. Res. Bull. **10**, 85 (1975)
38. H. Watanabe, J. Phys. Chem. Solids **25**, 1471 (1964)
39. E. Simanck, K.A. Muller, J. Phys. Chem. Solids **31**, 1027 (1970)
40. J.A. Weil, J.R. Bolton, J.E. Wertz, *Electron Paramagnetic Resonance-Elementary Theory and Practical Applications*, (Wiley, New York, 1994), p. 498
41. N.W. Aschcroft, N.D. Mermin, *Solid State Physics* (Harcourt College Publishers, 2001), p. 656
42. A.F. Wells, *Structural Inorganic Chemistry* (Clarendon, Oxford, 1984), pp. 592–597
43. O. Muller, R. Roy, *The Major Ternary Structural Families* (Springer, New York, 1974), pp. 38–47
44. Yu.B. Rozenfeld, S.R. Rotman, Phys. Stat. Solidi A **139**, 249 (1993)
45. J.M. Bunch, Phys. Rev. B **16**, 724 (1977)
46. K. Chakrabarthi, J. Phys. Chem. Solids **49**, 1009 (1988)
47. V.A. Adrichuk, L.G. Volzhenskaya, Yu.M. Zakharko, Yu.V. Zorenko, Zh. Prikl, Spektroskopia **47**, 3 (1987)
48. B.D. Evans, M. Stapelbroek, Phys. Rev. B **18**, 7089 (1978)
49. G.H. Rosenblatt, M.W. Rowe, G.P. Williams Jr., R.T. Williams, Phys. Rev. B **39**, 10309 (1989)
50. M.Kh. Ashurov, A.F. Rakov, R.A. Erzin, Solid State Commun. **120**, 491 (2001)